

Detection of Effective Porosity and Permeability Zoning in an Iranian Oil Field Using Fractal Modeling

Ardalan Kianersi^a, Ahmad Adib^a, Peyman Afzal^{a,*}

^a Department of Petroleum and Mining Engineering, South Tehran Branch, Islamic Azad University, Tehran, Iran

Article History:

Received: 03 April 2019,

Revised: 18 May 2019,

Accepted: 26 May 2019.

ABSTRACT

Identification and delineation of different zones in oil fields are among the fundamental tasks in petroleum explorations. Fractal methods are useful tools for such purposes. The aim of this paper is to conduct a comparative study of Concentration-Area (C-A) and Number-Size (N-S) fractal models to separate effective porous and permeable zones based on core logging samples collected from one of the oilfields in southern Iran. However, permeability and porosity threshold values were calculated based on the C-A and N-S log-log plots. A comparison between the C-A and N-S fractal results showed that the C-A method is more compatible with reality, and it is capable of separating permeable and porous zones in this oilfield.

Keywords : Concentration-area (C-A); Effective porosity; Number-size (N-S); Permeability; Southern Iran

1. Introduction

Several studies have tried to estimate petroleum reservoir properties, such as permeability and porosity, based on well logging, seismic, or production data [1-3]. The purpose of petrophysical studies is to determine the zoning in a reservoir formation. Porosity, water and hydrocarbon saturations, and permeability are important parameters which should be examined in petrophysical assessments to understand the quality of the reservoir [2-3]. Different methods have been proposed for the interpretation and determination of these parameters, specifically effective porosity and permeability. These methods include Reservoir Quality Index (RQI) and Flow Zone Index (FZI) [2-4]. The modeling of permeability and effective porosity is important for improving the production of an oilfield. Furthermore, these parameters are important in reservoir modeling and simulation, as they influence the rate of hydrocarbon production, ultimate recovery, optimal placement of wells, pressure, and fluid contact evaluation [3-6]. Thus, proper determination of permeability and effective porosity is of paramount importance since they affect the economy of the whole venture of development and operation of an oilfield.

Detection of different zones for effective porosity and permeability in a studied oilfield is an important aim for petroleum exploration. Several methods have been proposed to explain it properly. Moving averages and probability plots are among the most traditional and easy ways to use statistical methods for characterizing the effective porosity and permeability zoning in a petroleum reservoir [5]. Statistical methods are only applicable to cases where exploratory data follow a normal or lognormal distribution, and they define thresholds as the sum of the mean and standard deviations. However, the normal distribution does not provide the only possible model of data distribution. Therefore, traditional methods based on classical statistics may fail to recognize the zones in a studied area [5-6].

These limitations can be solved using fractal and multifractal modelings. Fractal geometry is an important non-linear mathematical

technique that was first introduced by Mandelbrot (1983) and has been applied in different fields of geosciences since the 1980s [7-14]. One of the main applications of fractal geometry is calculating the threshold and separating different zones (porous and permeable zones in this scenario) based on the difference between their fractal dimensions [15-18]. Additionally, several fractal methods have been developed and applied in geochemical explorations, such as Number-Size (N-S) by Mandelbrot (1983), Concentration-Area (C-A) by Cheng et al. (1994), Concentration-Distance (C-D) by Li et al. (2003), and Concentration-Volume (C-V) by Afzal et al. (2011). The detection and description of zone properties, including effective porosity and permeability, can be conducted using fractal methods. Fractal models have already been used to investigate either the permeability or porosity of oil shale samples [19-24]. Fractals are considered by a scaling law, which relates two variables: the scale factor and the object being measured. This scaling relationship is described by a power-law function that, in turn, explains the inherent physical characteristics of the object being analyzed, such as porosity and permeability [16, 25-27]. Different geological processes can be explained based on variations in fractal dimensions obtained from the analysis of relevant data. On the other hand, regionalized variables, such as porosity and permeability, can be interpreted by fractal geometry based on self-similarity and data complexity [25, 28-29]. According to the limited size of the dataset and the close extension of the study area, the N-S and C-A methods are suitable for the current research. In this study, the N-S and C-A fractal models were applied for the separation of porous and permeable zones in an oil reservoir of southern Iran.

2. Methodology

2.1. Number-size (N-S) fractal model

The N-S model, originally established by Mandelbrot (1983), can be utilized to describe the distribution of geochemical populations without pre-processing the data. The N-S method was developed by Agterberg

* Corresponding author. E-mail address: p_afzal@azad.ac.ir (P. Afzal).

(1995), Zuo et al. (2009), Deng et al. (2010), Hassanpour and Afzal (2013), and Afzal et al. (2016). This model shows that there is a relationship between desirable attributes and their cumulative number of samples. The model is expressed by the following equation [25]:

$$N(\geq\rho)=F\rho^{-D}$$

Where, ρ represents regionalized variables (such as porosity and permeability), $N(\geq\rho)$ denotes the cumulative number of samples with concentration values greater than or equal to ρ , F is a capacity constant, and D shows the scaling exponent or the fractal dimension of the distribution of the studied regionalized variable. Fractal dimensions can be positive, negative, complex, or fuzzy values. Based on the multifractal model proposed by Agterberg (1995), a power-law frequency model has been proposed to describe the N-S relationship according to the frequency distribution of element concentrations and the cumulative number of samples with those attributes [11, 14, 29-33].

According to Mandelbrot (1983), plotting the cumulative number against concentration in the log-log coordinates of $N(\geq\rho)$ versus $\log \rho$, which represents straight line segments with different slopes $-D$ corresponds to various concentration intervals. This method is suitable for low volume datasets, such as this case study.

2.2. Concentration-area (C-A) fractal model

The C-A model is developed based on the relationship between the obtained results and the exploratory data plus their surface area. Its advantages include easy implementation and the ability to compute quantitative thresholds for different zones [3, 9-10, 32, 34-37]. The C-A method, originally proposed by Cheng et al. (1994), is based on a simple empirical set of equations, which will be shortly presented. The C-A fractal model has the following general form:

$$A(\rho \leq v) \approx \rho^{-\alpha_1}; A(\rho \geq v) \approx \rho^{-\alpha_2}$$

Where, ρ and $A(\rho)$ reveal the studied attributes such as porosity/permeability and area with concentration values greater than the contour value ρ , respectively. Also, v represents the threshold values for this attribute, and $-\alpha_1$ and $-\alpha_2$ are fractal dimensions that are greater than zero [18, 26, 36, 38]. Fractal dimensions are calculated from the slopes of the straight lines in a log-log plot of $A(\rho)$ versus ρ .

Cheng et al. (1994) used two methodologies to calculate $A(\rho)$, as follows: (1) $A(\rho)$ is the area enclosed by contour level q on a contour map (e.g., porosity and permeability in this scenario), resulting from the estimation of raw data using a weighted moving average method such as ordinary kriging; and (2) $A(\rho)$ are the values derived via box-counting

of original values. By box-counting, one superimposes a grid with cells on the studied area. The $A(\rho)$ of a given q is equal to the number of cells multiplied by the cell area with concentration values greater than ρ . The average concentration values are utilized for those boxes containing more than one sample. Area-concentration $[A(\rho)]$ with concentrations greater than ρ usually represents a power-law relationship [9-10]. The breaks between straight-line segments on this plot and the corresponding values of ρ have been used as threshold values to discriminate values into different components, showing various factors, especially geological processes [39].

3. Results and Discussion

3.1. Dataset

The dataset comprises the physical properties of 364 core logging samples collected from a drilling borehole in an oilfield in southern Iran. The available data were recorded from horizontal and vertical core samples at 20cm intervals, and included effective porosity and permeability from depths 3500 m to 3700 m. The samples were analyzed under ambient, 800 psi, 3000 psi, and 6000 psi pressure circumstances. The N-S and C-A fractal methods were performed to detect porous and permeable zones in the oilfield. The data were gridded and estimated by the Ordinary Kriging (OK) method. The estimated data were used for fractal analysis through the C-A fractal method.

3.2. C-A application

The C-A log-log plots were generated for porosity and permeability at 800 psi, 3000 psi, and 6000 psi (Figs. 1 and 2). Permeability had six populations at ambient, 3000, and 6000 psi, but five populations at 800 psi. There was a multifractal nature for permeability and porosity in this area, based on different log-log plots, as depicted in Figs. 1 and 2. The major permeable zones at ambient, 800, 3000, and 6000 psi commenced from 138, 60.25, 54.95, and 47.86 md, respectively. These zones with high permeability values are located in the NE and SW parts of the area, as depicted in Figs. 3 and 4. Porosity populations were delineated based on the C-A log-log plots (Fig. 2), with the main porous zones beginning from 13-14%. There are seven populations for porosity ambient and six populations for others, as depicted in Fig. 2. Based on the fractal modeling, porous zones are situated in the SW and NE parts of the studied region, as displayed in Figs. 5 and 6. The threshold values for permeability and porosity are indicated in Table 1.

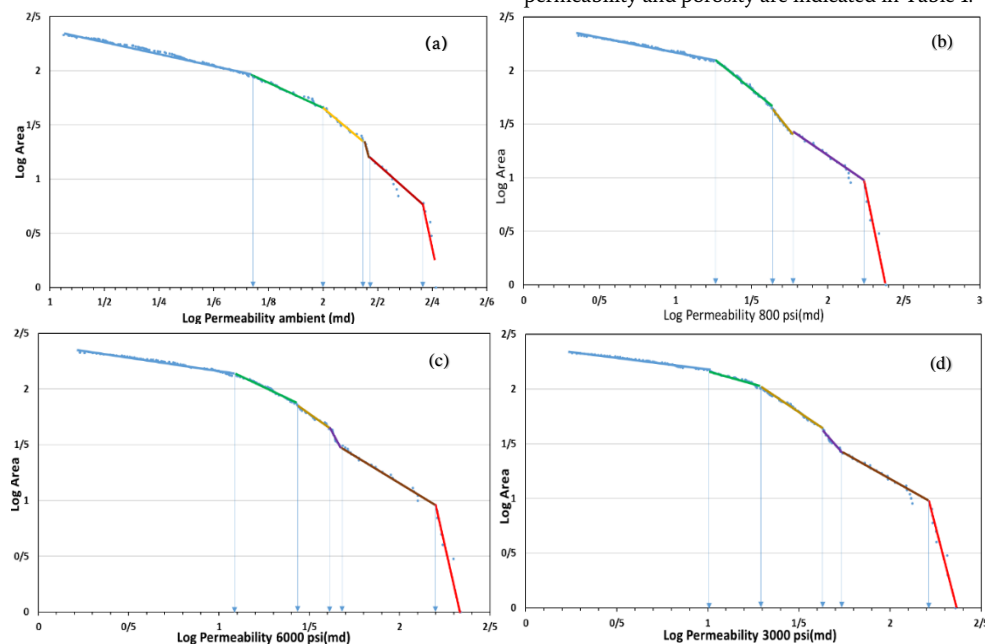


Fig. 1. The permeability log-log plots based on the C-A fractal model of the estimated data: (a) permeability at ambient; (b) permeability at 800 psi; (c) permeability at 3000 psi; and (d) permeability at 6000 psi.

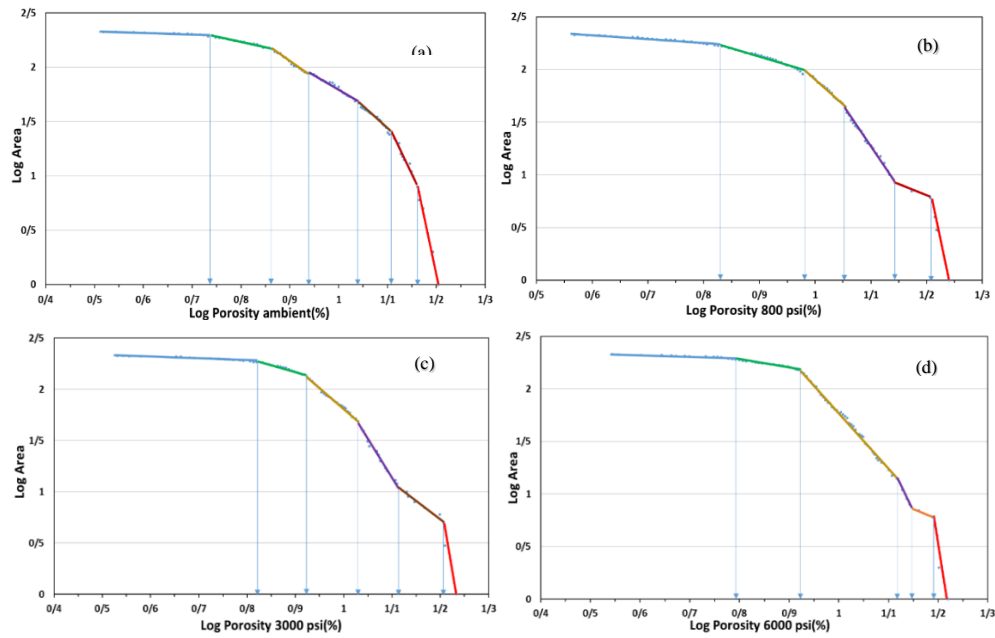


Fig. 2. The porosity log-log plots based on the C-A fractal model of the estimated data: (a) porosity at ambient; (b) porosity at 800 psi; (c) porosity at 3000 psi; and (d) porosity at 6000 psi.

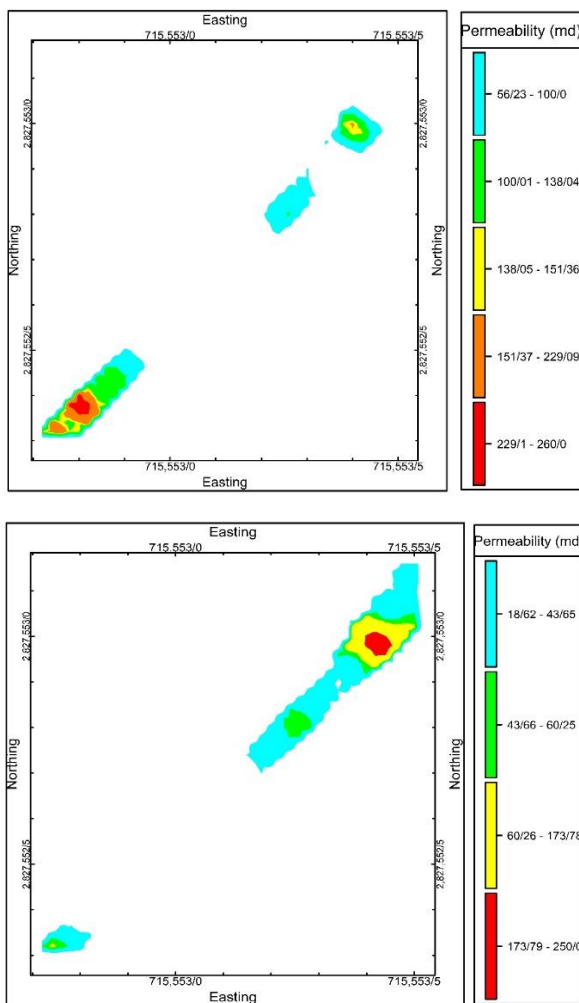


Fig. 3. Permeable zones distribution maps based on the C-A fractal method: (a) permeability at ambient; (b) permeability at 800 psi.

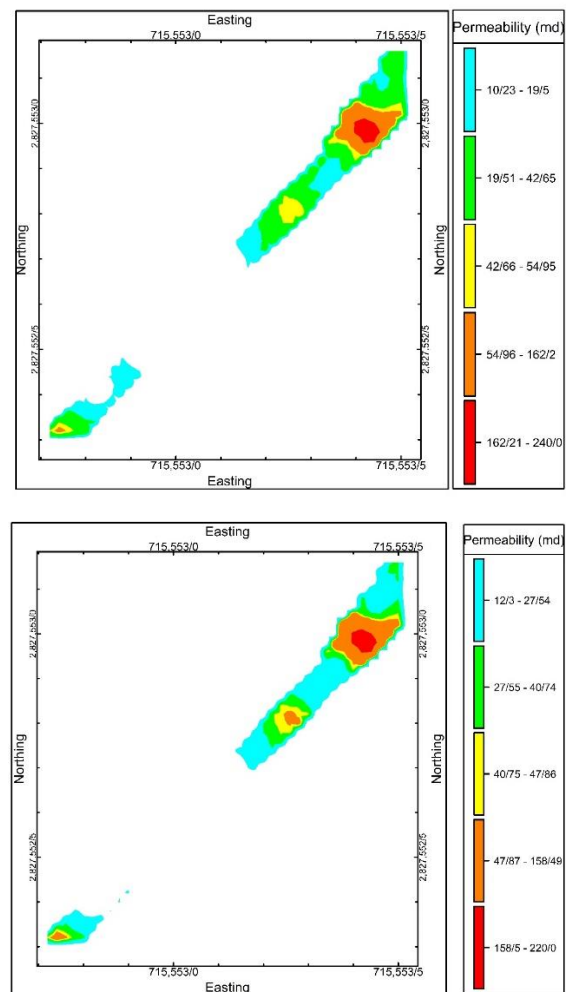


Fig. 4. Permeable zones distribution maps based on the C-A fractal method: (a) permeability at 3000 psi; (b) permeability at 6000 psi.

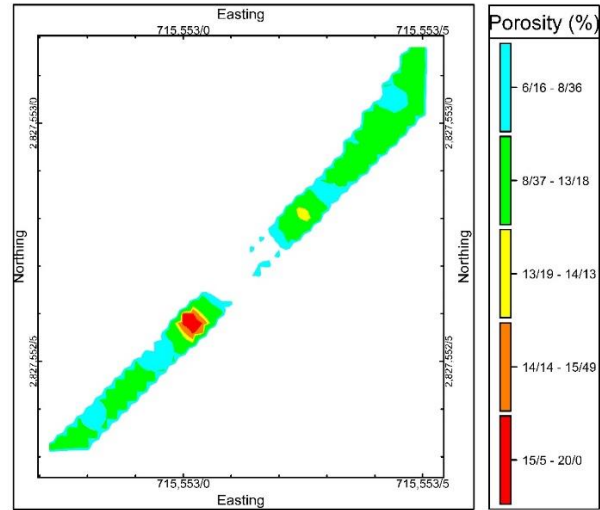
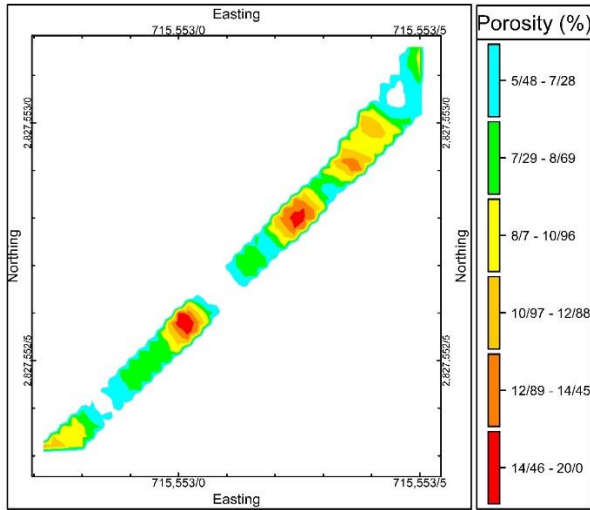


Fig. 6. Porous zones distribution maps based on the C-A fractal method: (a) porosity at 3000 psi; (b) porosity at 6000 psi.

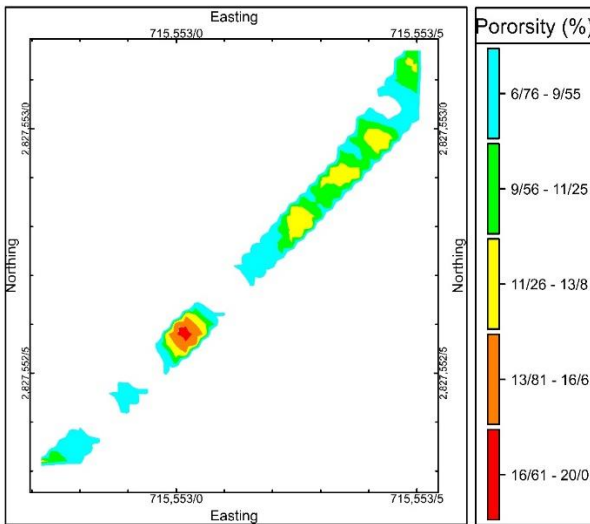
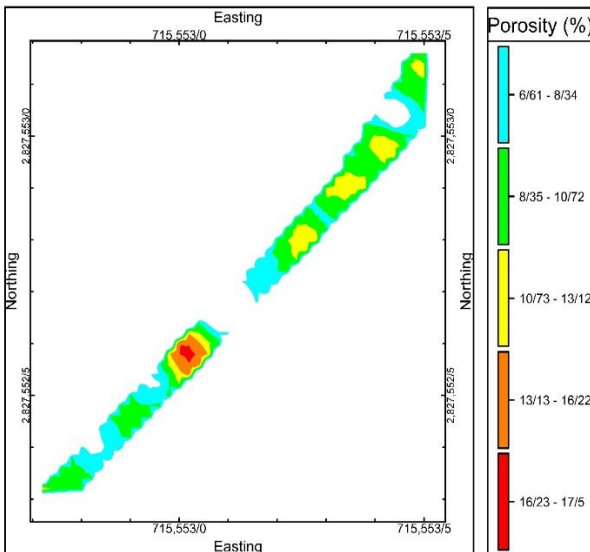


Table 1. Threshold values of permeable and porous zones in the studied area defined from the C-A fractal model (Figs. 1 and 2).

Qualification	Permeable & porous zones	Permeability range (md)	Porosity range (%)
Ambient	Background	<56.23	<5.48
	Weakly	56.23-100	5.48-7.28
	Moderately	100-138.04	7.28-8.69
	Highly	138.04-151.36	8.69-10.96
	Extremely	151.36-229.09	10.96-14.45
800 psi	Background	<18.62	<6.76
	Weakly	18.62-43.65	6.76-9.55
	Moderately	43.65-60.25	9.55-11.25
	Highly	60.25-173.78	11.25-13.8
	Extremely	173.78-241.5	13.8-16.6
3000 psi	Background	<10.23	<6.61
	Weakly	10.23-19.5	6.61-8.34
	Moderately	19.5-42.66	8.34-10.72
	Highly	42.66-54.95	10.72-13.12
	Extremely	54.95-162.18	13.12-16.22
6000 psi	Background	<12.3	<6.17
	Weakly	12.3-27.54	6.17-8.36
	Moderately	27.54-40.74	8.36-13.18
	Highly	40.74-47.86	13.18-14.13
	Extremely	47.86-158.49	14.13-15.49

Fig. 5. Porous zones distribution maps based on the C-A fractal method: (a) porosity at ambient; (b) porosity at 800 psi.



3.3. N-S implementation

The N-S method was conducted on the pre-treatment data without any estimations. The log-log plots of porosity and permeability were established under various conditions at 800 psi, 3000 psi, 6000 psi, and ambient (Figs. 7 and 8). Accordingly, the obtained results indicate that permeability at 800 psi, 3000 psi, and 6000 psi has five populations, but seven populations under an ambient condition. The highly permeable zones from the N-S fractal at ambient, 800 psi, 3000 psi, and 6000 psi began from 199.53, 158.49, and 100 md, respectively. As revealed in Figs. 9 and 10, these permeable zones with high values at 800 psi, 3000 psi, and 6000 psi are located in the NE, while under the ambient condition, they exist in the SW parts of the area. Based on the porosity log-log plots derived from the N-S fractal method, six populations under the ambient condition, five populations at 800 psi and 3000 psi, and four populations at 6000 psi were identified. Also, the obtained results suggest that the highly porous zones from the N-S method are located in the SW and NE of the area (Figs. 11 and 12). The high values of the porous zones from the N-S fractal started from 15-16%. Finally, the threshold values of porosity and permeability are provided in Table 2.

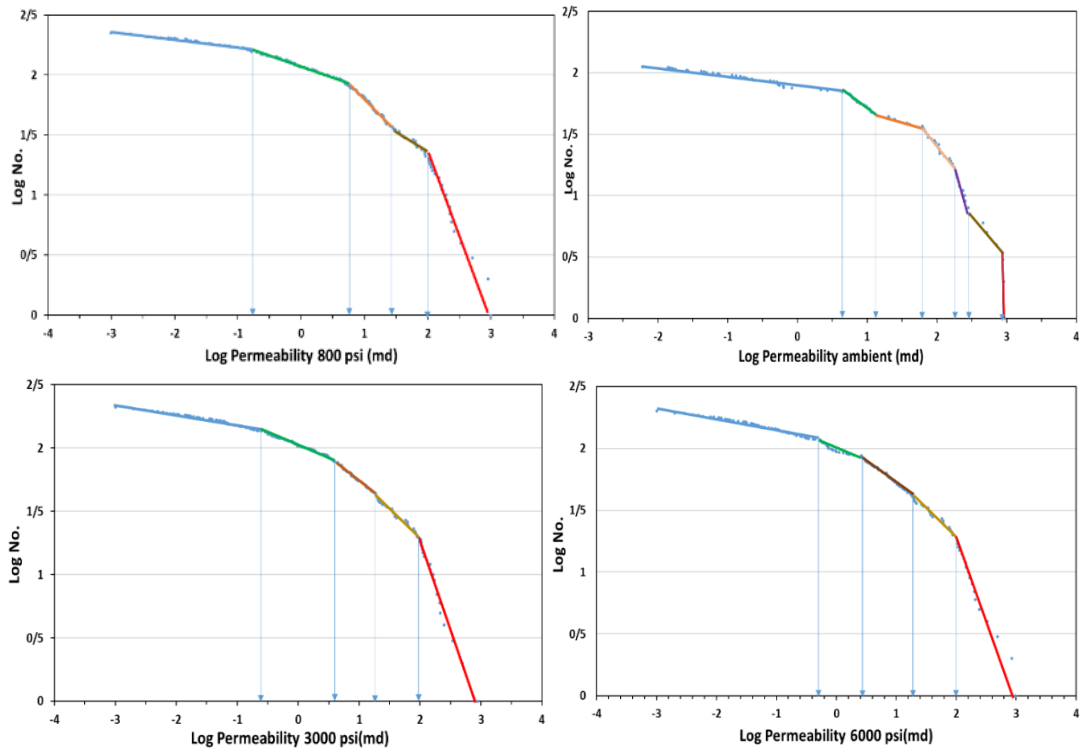


Fig. 7. The permeability log-log plots based on the N-S fractal model of data: (a) permeability at ambient; (b) permeability at 800 psi; (c) permeability at 3000 psi; and (d) permeability at 6000 psi.

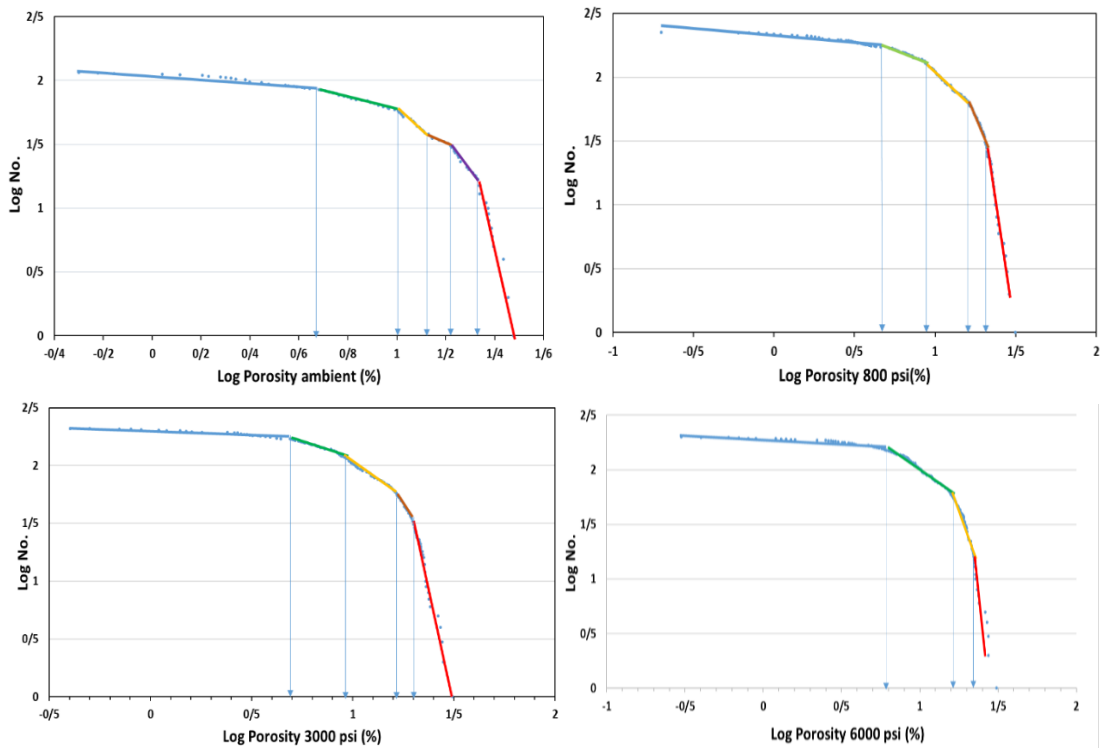


Fig. 8. The porosity log-log plots based on the N-S fractal model of data: (a) porosity at ambient; (b) porosity at 800 psi; (c) porosity at 3000 psi; and (d) porosity at 6000 psi.

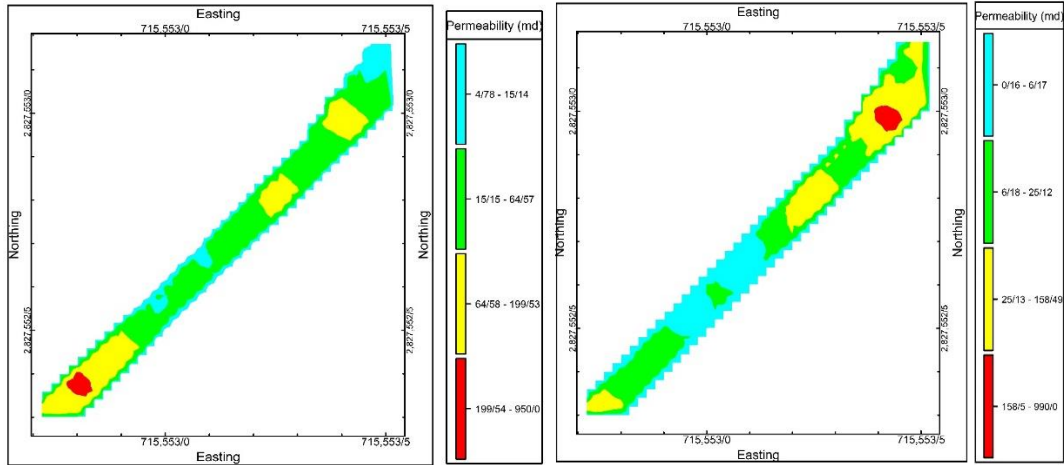


Fig. 9. Permeable zones distribution maps based on the N-S fractal method: (a) permeability at ambient; (b) permeability at 800 psi.

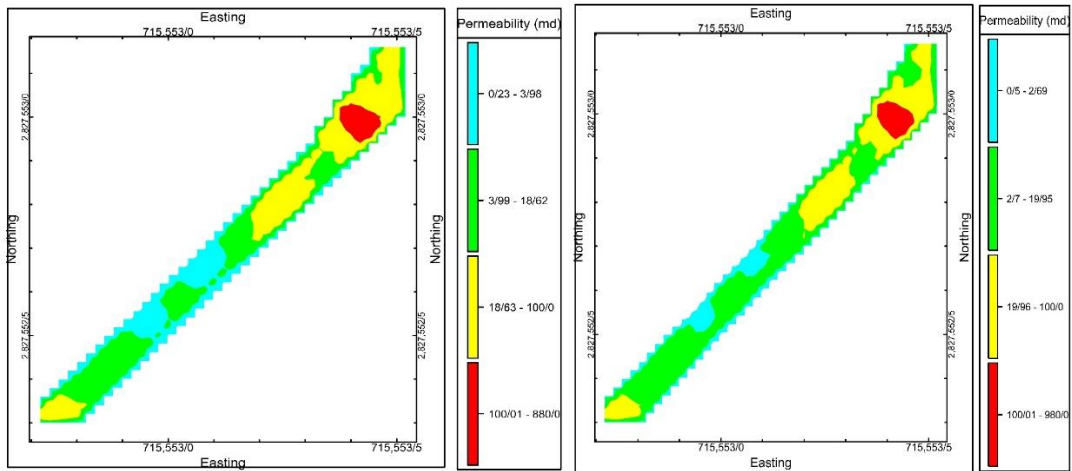


Fig. 10. Permeable zones distribution maps based on the N-S fractal method: (a) permeability at 3000 psi; (b) permeability at 6000 psi.

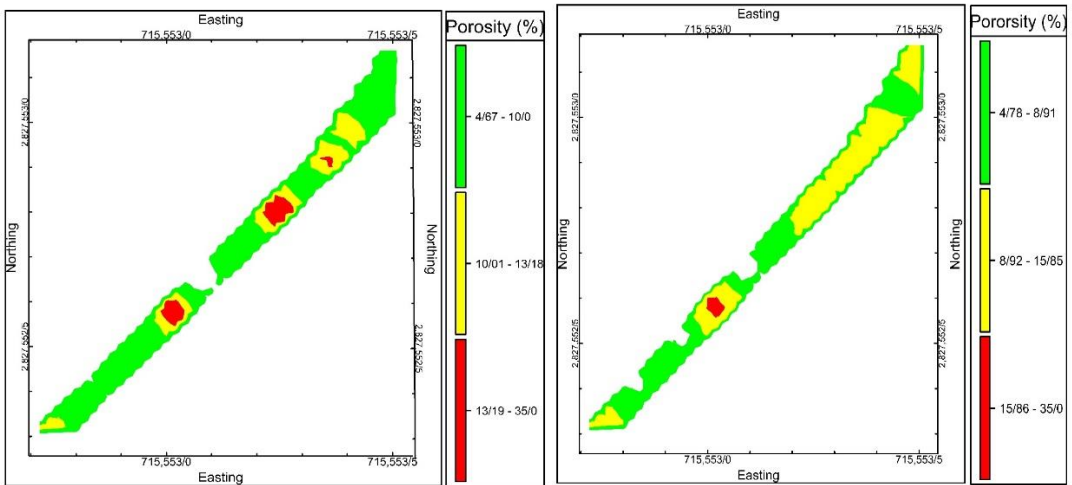


Fig. 11. Porous zones distribution maps based on the N-S fractal method: (a) porosity at ambient; (b) porosity at 800 psi.

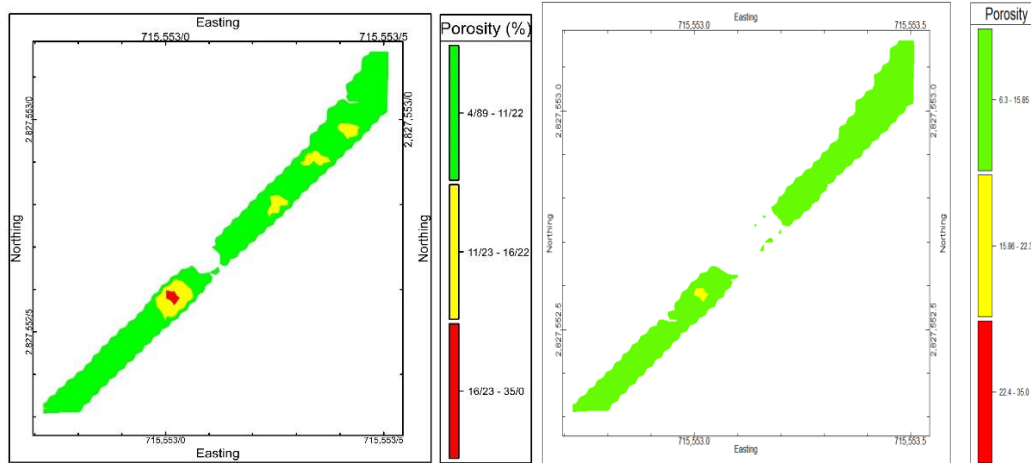


Fig. 12. Porous zones distribution maps based on the N-S fractal method: (a) porosity at 3000 psi; (b) porosity at 6000 psi.

Table 2. Threshold values of the permeable and porous zones in the studied area defined from the N-S fractal model (Figs. 7 and 8).

Qualification	Permeable & porous zones	Permeability range (md)	Porosity range (%)
Ambient	Background	<4.77	<4.68
	Weakly	4.77-15.14	4.68-10
	Moderately	15.14-64.56	10-13.18
	Highly	64.56-199.53	13.18-16.6
	Extremely	199.53-794.33	16.6-20.89
800 psi	Background	<0.16	<4.79
	Weakly	0.16-6.17	4.79-8.91
	Moderately	6.17-25.12	8.91-15.85
	Highly	25.12-158.49	15.85-19.95
	Extremely	158.49-389.04	19.95-31.5
3000 psi	Background	<0.23	<4.9
	Weakly	0.23-3.98	4.9-11.22
	Moderately	3.98-18.62	11.22-16.22
	Highly	18.62-100	16.22-20.42
	Extremely	100-875	20.42-31.1
6000 psi	Background	<0.5	<6.31
	Weakly	0.5-2.69	6.31-15.85
	Moderately	2.69-19.95	15.85-22.39
	Highly	19.95-100	22.39-30.8
	Extremely	100-971	>30.8

3.4. Correlation between fractal results and actual values

Carranza (2011) presented an analytical technique for the calculation of overlaps or spatial correlation between two binary models. Therefore, according to the overlaps between the numbers of cells in the fractal model and the cells existing in the conventional model (e.g., geological, actual, or standard models), a log-ratio matrix was established as Table 3.

Table 3. The log-ratio matrix to compare the performance of fractal modeling results with the conventional model (reality). A, B, C, and D represent the number of voxels in overlaps between classes in the binary geological model and the binary results of fractal models [40].

	Conventional model (Reality)	
	Inside zone	Outside zone
Fractal model	Inside zone	True positive (A) False positive (B)
	Outside zone	False negative (C) True negative (D)
Overall accuracy (OA) = (A+D)/(A+B+C+D)		

Where, (A) denotes the number of voxels that exist either in the fractal model or the conventional model; (B) represents the number of voxels in the fractal model but not available in the geological model; (C)

is the number of voxels embedded in the conventional model but not found in the fractal model; (D) is the number of voxels existing neither in the fractal nor in the conventional model; and (OA) is the main criterion for the evaluation of coincidence between the fractal results and the actual values. An intersection operation between a fractal zone model (porosity and permeability, in this scenario) and different zones in the conventional model was performed to obtain the number of cells corresponding to each of the four classes of overlapping zones, as shown in Table 5. In this study, porous and permeable zones were compared with standard zones presented by Tiab and Donaldson (2004) [41].

3.5. Comparison between permeability fractal results and actual results

A comparison between N-S and C-A permeability fractal results was performed using the log-ratio matrix. A standard range of permeability (50-150 md) was chosen for the conventional model [41]. Further, permeability fractal ranges in different conditions were selected considering their threshold values. As depicted in Tables 4-7, it can be concluded that the C-A fractal method has greater accuracy and is closer to reality. The OAs obtained by the C-A are higher than those by the N-S modeling for different ranges. The OAs resulting from the C-A model are higher than 96% in various zones, but these values for the N-S method are between 90%-95%, as depicted in Tables 4-7. The difference between C-A and N-S modeling is near to 10% and 7% for permeability at 3000 psi and 6000 psi, respectively (Tables 6-7).

Table 4. Comparison between the results derived from the N-S and C-A fractal models (permeability under the ambient condition).

		Standard (50-150 md)				
		Inside zone	Outside zone			
N-S fractal Permeability ambient (64.56-199.52 md)	Inside zone	A	14	B	7	
	Outside zone	C	3	D	136	
			OA			0.9375
			Standard (50-150 md)			
		Inside zone	Outside zone			
C-A fractal Permeability ambient (100-138.04 md)	Inside zone	A	21	B	0	
	Outside zone	C	59	D	1765	
			OA			0.968022

Table 5. Comparison between the results derived from the N-S and C-A fractal models (permeability at 800 psi).

		Standard (50-150 md)				
		Inside zone	Outside zone			
N-S fractal Permeability ambient (64.56-199.52 md)	Inside zone	A	15	B	11	
	Outside zone	C	0	D	236	
			OA			0.958015
			Standard (50-150 md)			
		Inside zone	Outside zone			
C-A fractal Permeability ambient (100-138.04 md)	Inside zone	A	17	B	0	
	Outside zone	C	8	D	1820	
			OA			0.995664

Table 6. Comparison between the results derived from the N-S and C-A fractal models (permeability at 3000 psi).

		Standard (50-150 md)			
		Inside zone		Outside zone	
N-S fractal	Inside zone	A	8	B	16
Permeability ambient	Outside zone	C	9	D	229
(64.56-199.52 md)		OA	0.90458		
		Standard (50-150 md)			
		Inside zone		Outside zone	
C-A fractal	Inside zone	A	18	B	0
Permeability ambient	Outside zone	C	5	D	1822
(100-138.04 md)		OA	0.99729		

Table 7. Comparison between the results derived from the N-S and C-A fractal models (permeability at 6000 psi).

		Standard (50-150 md)			
		Inside zone		Outside zone	
N-S fractal	Inside zone	A	9	B	10
Permeability ambient	Outside zone	C	8	D	236
(64.56-199.52 md)		OA	0.931559		
		Standard (50-150 md)			
		Inside zone		Outside zone	
C-A fractal	Inside zone	A	21	B	2
Permeability ambient	Outside zone	C	0	D	1822
(100-138.04 md)		OA	0.998916		

3.6. Comparison between porosity fractal results and actual values

The N-S and C-A fractal results for porosity zones were evaluated using the log-ratio matrix, with its conclusions exhibited in Tables 8-11. In this comparison, a range of 10-15% was assumed for the standard porosity range [41]. Porosity fractal ranges were selected based on their threshold values derived from the N-S and C-A fractal models. According to the obtained results, under the conditions of ambient, 800 psi, 3000 psi, and 6000 psi, the C-A fractal method presented a more accurate response than the N-S fractal method. The OAs derived via the C-A were higher than those found by the N-S modeling for different ranges. The OAs resulting from the C-A model were equal to 98% in different zones, but these values for the N-S model lay within the range 76%-92%, as reported in Tables 8-11. The difference between C-A and N-S modelings is 21% for 6000 psi (Tables 11). In addition, the difference for 800 psi and 3000 psi is 6% and 8%, respectively (Tables 9-10).

Table 8. Comparison between the results derived from the N-S and C-A fractal models (porosity under the ambient condition).

		Standard (10 – 15%)			
		Inside zone		Outside zone	
N-S fractal	Inside zone	A	20	B	0
Permeability ambient	Outside zone	C	5	D	127
(64.56-199.52 md)		OA	0.967105		
		Standard (10 – 15%)			
		Inside zone		Outside zone	
C-A fractal	Inside zone	A	25	B	0
Permeability ambient	Outside zone	C	38	D	1782
(100-138.04 md)		OA	0.979404		

Table 9. Comparison between the results derived from the N-S and C-A fractal models (porosity at 800 psi).

		Standard (10 – 15%)			
		Inside zone		Outside zone	
N-S fractal	Inside zone	A	42	B	19
Permeability ambient	Outside zone	C	0	D	195
(64.56-199.52 md)		OA	0.925781		
		Standard (10 – 15%)			
		Inside zone		Outside zone	
C-A fractal	Inside zone	A	40	B	0
Permeability ambient	Outside zone	C	39	D	1766
(100-138.04 md)		OA	0.978862		

Table 10. Comparison between the results derived from the N-S and C-A fractal models (porosity at 3000 psi).

		Standard (10 – 15%)			
		Inside zone		Outside zone	
N-S fractal	Inside zone	A	23	B	9
Permeability ambient	Outside zone	C	15	D	198
(64.56-199.52 md)		OA	0.902041		
		Standard (10 – 15%)			
		Inside zone		Outside zone	
C-A fractal	Inside zone	A	39	B	0
Permeability ambient	Outside zone	C	28	D	1778
(100-138.04 md)		OA	0.984824		

Table 11. Comparison between the results derived from the N-S and C-A fractal models (porosity at 6000 psi).

		Standard (10 – 15%)			
		Inside zone		Outside zone	
N-S fractal	Inside zone	A	36	B	56
Permeability ambient	Outside zone	C	0	D	146
(64.56-199.52 md)		OA	0.764706		
		Standard (10 – 15%)			
		Inside zone		Outside zone	
C-A fractal	Inside zone	A	7	B	0
Permeability ambient	Outside zone	C	50	D	1788
(100-138.04 md)		OA	0.9729		

4. Conclusion

This study was conducted on a drilling borehole of an oilfield from the south of Iran. It presented the specific use of N-S and C-A fractal methods for the separation of permeable and porous zones as a useful tool for petro-physical exploration. The advantages of these methods include simplicity and straightforward computational implementations. Both of the N-S and C-A fractal models revealed the highly porous and permeable zones. The results obtained by fractal modeling suggested that the main zones for petroleum extraction occur in the SW and NE parts of the area. The threshold values for highly permeable zones at ambient, 800 psi, 3000 psi, and 6000 psi began from 138, 60.25, 54.95, and 47.86 md based on the C-A fractal model, respectively. Also, the major permeable zones derived from the N-S fractal method at ambient, 800, 3000, and 6000 psi started from 199.53, 158.49, and 100 md in order and priority. According to the obtained porosity log-log plots, the threshold values for the major porous zones began from 14.5% as the average value for both of the C-A and N-S fractal models. A comparison between the C-A and N-S fractal results revealed that under various conditions of ambient, 800, 3000, and 6000 psi, the C-A fractal method outperforms the N-S fractal method. Consequently, the permeability and porosity results derived from the C-A fractal model has a better equivalence with the reality; therefore, it is more capable of separating the porous and permeable zones in petroleum extractions.

REFERENCES

- [1] Anifowose, F., Adeniyi, S., Abdurraheem, A., Alshohail, A. (2016) 'Integrating seismic and log data for improved petroleum reservoir properties estimation using non-linear feature-selection based hybrid computational intelligence models', Journal of Petroleum Science and Engineering, Vol. 145, pp.230-237.
- [2] Ebrahimi H., Kamkar Rouhani A., Soleimani Monfared M. (2018) 'Introduction of Developed Reservoir Quality Index in Characterization of Hydrocarbon Reservoirs, Study of Kangan Formation in one of Fields in South of Iran' Petroleum Research, Vol. 28, pp. 44-48.
- [3] Worthington P. F. (2008) 'The application of cutoffs in integrated reservoir studies' SPE Reservoir Evaluation & Engineering, Vol. 11, No. 6, pp. 968-975.
- [4] Nabawy, B.S., and Al-Azazi, N.A. (2015) 'Reservoir zonation and

- discrimination using the routine core analyses data: the upper Jurassic Sab'atayn sandstones as a case study, Sab'atayn basin, Yemen' *Arabian Journal of Geosciences*, Vol. 8, pp. 5511-5530.
- [5] Liu, M., Ostadhassan, M. (2017) 'Multi-scale fractal analysis of pores in shale rocks', *Journal of Applied Geophysics*, Vol. 140, pp. 20-28.
- [6] Davis, J.C. (2002) 'Statistics and data analysis in geology' (3th ed.), John Wiley & Sons Inc., New York, pp.656.
- [7] Mandelbrot, B. (1983) 'The fractal geometry', Freeman, New York, pp.1-468.
- [8] Geng, L., Li, G., Zitha, P., Tian, S., Sheng, M. (2016) 'A fractal permeability model for shale gas flow through heterogeneous matrix systems', *Journal of Natural Gas Science and Engineering*, Vol. 35, pp.593-604.
- [9] Miao, T., Long, Z., Chen, A., Yu, B. (2017) 'Analysis of permeability for slug flow in fractal porous media', *International Communications in Heat and Mass Transfer*, Vol. 88, pp.194-202.
- [10] Cheng, Q., Agterberg, F.P., Ballantyne, S.B. (1994) 'The separation of geochemical anomalies from background by fractal methods', *Journal of Geochemical Exploration*, Vol. 51, pp.109-130.
- [11] Afzal, P., Khakzad, A., Moarefvand, P., Rashidnejad Omran, N., Esfandiari, B., Fadakar Alghalandis, Y., (2010) 'Geochemical anomaly separation by multifractal modeling in Kahang (Gor Gor) porphyry system, Central Iran, *Journal of Geochemical Exploration* Vol. 104, pp.34-46.
- [12] Afzal, P., Ahmadi, K., Rahbar, K. (2017) 'Application of fractal-wavelet analysis for separation of geochemical anomalies', *Journal of African Earth Sciences*, Vol. 128, pp.27-36.
- [13] Daneshvar Saein, L. (2017) 'Delineation of enriched zones of Mo, Cu and Re by concentration-volume fractal model in Nowchun Mo-Cu porphyry deposit, SE Iran', *Iranian Journal of Earth Sciences*, Vol. 9(1), pp. 64-72.
- [14] Wang, Y., Wu, C., Zhu, Y., Chen, Sh., Liu, Sh., and Zhang, R. (2018) 'Morphology and fractal characterization of multiscale pore structures for organic-rich lacustrine shale reservoirs', *Fractals*, Vol. 26, 1840013.
- [15] Karami, K. and Afzal, P. (2015) 'Application of multifractal modeling for separation of sulfidic mineralized zones based on induced polarization and resistivity data in the Ghare-Tappeh Cu deposit, NW Iran', *Iranian Journal of Earth Sciences*, Vol. 7, pp.134-141.
- [16] Afzal, P., Fadakar Alghalandis, Y., Khakzad, A., Moarefvand, P., Rashidnejad Omran, N., (2011) 'Delineation of mineralization zones in porphyry Cu deposits by fractal concentration-volume modeling', *Journal of Geochemical Exploration*, Vol. 108, pp.220-232.
- [17] Abdideh, M., Rezaee, H. (2017) 'Separation of rock types in reservoir rock using concentration-area multifractal model', *Geosystem Engineering*, Vol. 20, pp. 348-354.
- [18] Adib, A., Afzal, P., Mirzaei, S., Aliyari, F. (2017) 'Determination of the relationship between major fault and zinc mineralization using fractal modeling in the Behabad fault zone, Central Iran', *Journal Of African Earth Sciences*, Vol. 134, pp.319-308.
- [19] Yu, B., Cheng, P. (2002) 'A fractal permeability model for bi-dispersed porous media', *International Journal of Heat & Mass Transfer*, 45 (14), 2983-2993.
- [20] Cai, Y., Liu, D., Pan, Z., Yao, Y., Li, J., Qiu, Y. (2013) 'Pore structure and its impact on CH₄ adsorption capacity and flow capability of bituminous and subbituminous coals from Northeast China', *Fuel*, Vol. 103, pp.258-268.
- [21] Yang, F., Ning, Z., Liu, H. (2014) 'Fractal characteristics of shales from a shale gas reservoir in the Sichuan Basin, China', *Fuel* 115, 378-384.
- [22] Xu, P. (2015) 'A discussion on fractal models for transport physics of porous media', *Fractals*, Vol. 23, 1530001.
- [23] Xu, P., Li, C., Qiu, S., and Pulung Sasmito, A. (2016) 'A fractal network model for fractured porous media', *Fractals*, Vol. 24, 1650018.
- [24] Liu, R., Yu, L., Jiang, Y., Wang, Y., Li, B. (2017) 'Recent developments on relationships between the equivalent permeability and fractal dimension of two-dimensional rock fracture networks', *Journal of Natural Gas Science and Engineering*, Vol. 45, pp.771-785.
- [25] Afzal, P. (2014) 'Classification of Coking Coals in C1 Seam of East-Parvadeh Coal Deposit, Central Iran Using Multifractal Modeling' *Iranian Journal of Earth Sciences*, Vol. 6, pp. 108-113.
- [26] Huang, H., L., Chen, Sun, W., Xiong, F., Jingkun Jia, W.J., Tang, X., Zhang, Sh., Gao, J., and Luo, B. (2018) 'Pore-throat structure and fractal characteristics of Shihezi formation tight gas sandstone in the Ordos basin, China', *Fractals*, Vol. 26, 1840005.
- [27] Li, K., Zeng, F., Cai, J., Sheng, G., Xia, P., and Zhang, K. (2018) 'Fractal characteristics of pores in Taiyuan formation shale from Hedong coal field, China', *Fractals*, Vol. 26, 1840006.
- [28] Agterberg, F. P. (1995) 'Multifractal modeling of the sizes and grades of giant and supergiant deposits', *International Geology Review*, 37(1), 1-8.
- [29] Turcotte, D.L. (1997) 'Fractals and chaos in geology and geophysics', Cambridge University Press, Cambridge.
- [30] Zuo, R., Cheng, Q. and Xia, Q. (2009) 'Application of fractal models to characterization of vertical distribution of geochemical element concentration', *Journal of Geochemical Exploration*, Vol. 102, pp.37-43.
- [31] Sadeghi, B., Afzal, P., Moarefvand, P., Khodashenas, N. (2012) 'Application of concentration-area fractal method for determination of Fe geochemical anomalies and the background in Zaghia area, Central Iran', 34th International Geological Congress (IGC), Brisbane, Australia, pp 5-10.
- [32] Shamseddin Meigooni, M., Afzal, P., Gholinejad, M., Yasrebi, A.B., Sadeghi, B., (2014) 'Delineation of geochemical anomalies using factor analysis and multifractal modeling based on stream sediments data in Sarajeh 1: 100,000 sheet, Central Iran', *Arabian Journal of Geosciences*, Vol. 20, pp. 348-354.
- [33] Afzal, P., Mirzaei, M., Yousefi, M., Adib, A., Khalajmasoumi, M., Zia Zarifi, A., Foster, P. and Yasrebi, A.B. (2016) 'Delineation of geochemical anomalies based on stream sediment data utilizing fractal modeling and staged factor analysis', *Journal of African Earth Sciences*, Vol. 119, pp.139-149.
- [34] Nazarpour, A. (2018) 'Application of C-A fractal model and exploratory data analysis (EDA) to delineate geochemical anomalies in the: Takab 1:25,000 geochemical sheet, NW Iran', *Iranian Journal of Earth Sciences*, Vol. 10, pp. 173-180.
- [35] Lima, A., De Vivo, B., Cicchella, D., Cortini, M., Albanese, S. (2003) 'Multifractal IDW interpolation and fractal filtering method in environmental studies: an application on regional stream sediments of Italy, Campania region', *Applied*

Geochemistry, Vol. 18, pp. 1853–1865.

- [36] Adib, A., Afzal, P., Heydarzadeh, K. (2015) 'Site effect classification based on micro tremor data analysis using a concentration–area fractal model', *Nonlinear Processes in Geophysics*, Vol. 22, pp.53–63.
- [37] Khalajmasoumi, M., Sadeghi, B., Carranza, E.J.M., Sadeghi, M. (2017) 'Geochemical anomaly recognition of rare earth elements using multi-fractal modelling correlated with geological features, Central Iran', *Journal of Geochemical Exploration*, Vol. 181, pp. 318–332.
- [38] Zuo, R., Xia, Q., Zhang, D. (2013) 'A comparison study of the C-A and S-A models with singularity analysis to identify geochemical anomalies in covered areas', *Applied Geochemistry*, Vol. 33, pp.165–172.
- [39] Daya, A. A., Boomeri, M., & Mazraee, N. (2017) 'Identification of geochemical anomalies by using of concentration-area (C-A) fractal model in Nakhilab region, SE Iran', *International Journal of Mining and Mineral Engineering*, Vol. 8 (1), pp. 70.
- [40] Carranza, E.J.M. (2011) 'Analysis and mapping of geochemical anomalies using logratio transformed stream sediment data with censored values', *Journal of Geochemical Exploration*, Vol. 110, pp.167–185.
- [41] Tiab, D., Donaldson, EC. (2004) 'Petro-physics (2nd edition)', Elsevier.